Journal of Geodynamics 49 (2010) 181–189

Contents lists available at ScienceDirect

Journal of Geodynamics

journal homepage: http://www.elsevier.com/locate/jog

PS-InSAR processing methodologies in the detection of field surface deformation—Study of the Granada basin (Central Betic Cordilleras, southern Spain)

Joaquim J. Sousa[a,b,*], Antonio M. Ruiz[c], Ramon F. Hanssen[d], Luisa Bastos[a], Antonio J. Gil[c], Jesús Galindo-Zaldívar[e], Carlos Sanz de Galdeano[f]

[a] *Faculdade de Ciências da Universidade do Porto, Portugal*
[b] *Departamento de Matemática, Universidade de Trás-os-Montes e Alto Douro, Vila Real, Portugal*
[c] *Departamento de Ingeniería Cartográfica, Geodésica y Fotogrametría, Universidad de Jaén, Jaén, Spain*
[d] *Delft Institute of Earth Observation and Space Systems (DEOS), Delft University of Technology, Delft, The Netherlands*
[e] *Departamento de Geodinámica, Universidad de Granada, Granada, Spain*
[f] *Instituto Andaluz de Ciencias de la Tierra, Consejo Superior de Investigaciones Científicas-Universidad de Granada, Granada, Spain*

A R T I C L E I N F O

Article history:
Received 22 December 2008
Received in revised form 7 December 2009
Accepted 22 December 2009

Keywords:
PS-InSAR
Deformation
DePSI
StaMPS
Granada basin
Radar interferometry

A B S T R A C T

Differential SAR interferometry (DInSAR) is a very effective technique for measuring crustal deformation. However, almost all interferograms include large areas where the signals decorrelate and no measurements are possible. Persistent scatterer interferometry (PS-InSAR) overcomes the decorrelation problem by identifying resolution elements whose echo is dominated by a single scatterer in a series of interferograms.

Two time series of 29 ERS-1/2 and 22 ENVISAT ASAR acquisitions of the Granada basin, located in the central sector of the Betic Cordillera (southern Spain), covering the period from 1992 to 2005, were analyzed. Rough topography of the study area associated to its moderate activity geodynamic setting, including faults and folds in an uplifting relief by the oblique Eurasian–African plate convergence, poses a challenge for the application of interferometric techniques. The expected tectonic deformation rates are in the order of ~1 mm/yr, which are at the feasibility limit of current InSAR techniques.

In order to evaluate whether, under these conditions, InSAR techniques can still be used to monitor deformations we have applied and compared two PS-InSAR approaches: DePSI, the PS-InSAR package developed at Delft University of Technology (TU Delft) and StaMPS (Stanford Method for Persistent Scatterers) developed at Stanford University. Ground motion processes have been identified for the first time in the study area, the most significant process being a subsidence bowl located at the village of Otura.

The idea behind this comparative study is to analyze which of the two PS-InSAR approaches considered might be more appropriate for the study of specific areas/environments and to attempt to evaluate the potentialities and benefits that could be derived for the integration of those methodologies.

1. Introduction

In the late 1990s it was noticed that some radar targets maintain stable backscattering characteristics for a period of months or years (Usai, 1997; Usai and Hanssen, 1997), and the phase information from these stable targets (hereafter called Persistent Scatterers or PS) can be used, even over a long time period, profiting from a SAR scene archive in existence since 1991 (ERS-1) which allows the establishment of long time series of SAR images. This led to the development of Advanced Differential Interferometric Synthetic Aperture Radar (A-DInSAR) methodologies, adopting both amplitude stability and coherence stability (i.e. correlation) as pixel selection criteria. The choice of the selection criterion depends on the application at hand.

In this study only the amplitude stability selection criterion is addressed: Persistent Scatterer Interferometry (PS-InSAR), which enables the detection of earth surface deformation at the millimeter level (Ferretti et al., 2000, 2001).

These A-DInSAR techniques represent an outstanding advance with respect to the standard DInSAR, which often is the only one that can be implemented due to the limited data availability for many practical deformation measurement applications. For the ERS/Envisat satellites, DInSAR has the advantage of delivering high

* Corresponding author at: Alameda do Monte da Virgem 4430 V.N. Gaia, Portugal. Fax: +351 227861299.
E-mail address: jjsousa@utad.pt (J.J. Sousa).

0264-3707/$ – see front matter © 2010 Elsevier Ltd. All rights reserved.
doi:10.1016/j.jog.2009.12.002

ground resolution, 4×20 m, on a 100 km wide swath. It provides users with the capability of mapping and monitoring subtle changes of the ground surface with a precision of the order of 1 cm or less (Gabriel et al., 1989), but limited by temporal and geometric decorrelation and atmospheric inhomogeneities (Ferretti et al., 1999, 2001). However, these disturbances can be removed in advanced DInSAR approaches by means of stacking procedures of SAR images (Monti Guarnieri and Tebaldini, 2007).

Temporal decorrelation in our area of interest is caused by physical terrain changes between the images taken at different acquisition times. These changes affect the scattering characteristics of the surface, which results in a loss of coherence (Hanssen, 2001). In the InSAR technique, the same scene is imaged from different incidence angles due to the perpendicular baseline. This change of the incidence angle leads to a relative displacement between the range spectra of the two SAR images. Only the portion of spectrum common to both images is useful for generating an interferogram. This spectral shift explains the concept of critical baseline. If the spatial baseline is increased, the spectral shift is also increased. When this shift is so large that there are no common band frequencies the critical baseline has been reached, and the interferometric information is lost.

Atmospheric variations generate a change in the electric path, causing extra phase fringes to appear in the interferogram (Zebker et al., 1997). This interferometric phase component is known as atmospheric artifacts. Obviously, the atmospheric artifact is a disturbance signal, and therefore can be presented as a source of error that degrades the interferogram. It is most likely that conditions in the atmosphere are not identical as the images are acquired at different times. Therefore, the length of the measured ray-path between the sensor and the ground can change due to the time delay caused by tropospheric and ionospheric disturbances. This means that we have a greater number of phase cycles between the satellite and the ground target and as a result an absolute phase delay which is not uniform throughout the scene. Any atmospheric heterogeneity will appear as a phase distortion in an interferogram and thus limit the confidence of the results. Hanssen and Feijt (1996) quantitatively evaluate the atmospheric effects on SAR interferometry using an existing tropospheric model, deriving a quantitative assessment of the influence on the interferometric phase of three major atmospheric parameters: pressure, relative humidity and temperature.

According to Zebker et al. (1997), interferograms derived from repeat-pass radar interferometry can be affected by the time and space variation caused by atmospheric water vapour. Furthermore, variations of pressure and temperature do not induce significant distortion as they are more evenly distributed throughout an interferogram than water vapour in the troposphere. Zebker et al. (1997), state that dry regions have fewer variations than wet regions. Although night-time acquisition can reduce atmospheric artifacts more than daytime, due to more quiescent vegetation and the statistically more stable night-time atmosphere (Massonnet and Feigl, 1998), the user has no control over the acquisition time for any given region on the Earth.

We applied PS-InSAR in order to derive displacement information in the Granada basin area. The unfavourable conditions of the study area are caused by the rough topography and the weak deformation rates, which represent a challenge and an opportunity to test the limits of this technique. As a result of the PS processing, several interesting features were exposed which deserve a deeper investigation in order to understand and eventually relate these results to the present tectonic or anthropogenic processes in the area. Two PS-InSAR approaches are compared in order to further understand their potential.

The first, DePSI, the package for Persistent Scatterer Interferometry developed at TU Delft simultaneously estimates the deformation for each PS in order to estimate and remove nuisance terms, which requires a model for deformation over time. An initial set of PS pixels is identified by an analysis of their amplitude scintillations in a series of interferograms. The goal of this step is to estimate the atmospheric phase at these pixel positions in all interferograms. This is accomplished by filtering the residual phase after estimation of the modelled parameters, i.e. the DEM error and the displacement rate, taking advantage of the spatial correlation of the atmospheric signal. The estimations are performed between nearby points, because the phase contributions that are not modelled need to be smaller than π (since the observed data is not unwrapped), and the atmospheric signal is reduced considerably by this difference. This method works best in urban areas where man-made structures increase the likelihood of finding a non-fluctuating scatterer in any given pixel.

The second method, StaMPS (Stanford Method for Persistent Scatterers), uses both amplitude and phase analysis to determine the PS probability for individual pixels. First an initial selection based only on amplitude analysis is performed, and then the PS probability is refined using phase analysis in an iterative process. Once selected, the signal due to deformation in the PS pixels is isolated. In contrast to DePSI this method produces a time series of deformation, with no prior assumptions about the temporal nature of deformation. This is achieved by using the spatially correlated nature of deformation rather than requiring a known temporal dependence.

The different approaches (temporal vs. spatial assumptions) for the two techniques lead to complementary performance. The spatial smoothness assumption (StaMPS) is less affected by variations in the deformation rates, but may miss the detection of a single scatterer which behaves anomalously with respect to its surroundings. The temporal smoothness assumption (DePSI) seems more suitable for the detection of spatially variable (non-smooth) signals, but may fail to detect scatterers which have a highly variable deformation rate because of the targets detection criterion based on linear motion of the DePSI technique. Consequently, depending on the deformation characteristics, one of the two might be preferred over the other.

During this study significant differences in PS density and distribution were detected, motivating a comparative study in order to identify the main causes. We analyze which approach might be more appropriate for studying specific areas/environments and try to evaluate the potential and benefits which could be derived from the integration of these two methodologies.

2. Study area

The study area, situated in the Betic Cordillera (Spain, see Fig. 1), is located in the western part of the Mediterranean Sea, a region structured during the Alpine orogeny and affected by a complex geologic evolution (Sanz de Galdeano and Vera, 1992; Galindo-Zaldívar et al., 1993). The Betic Cordillera is superimposed over the wide deformation zone between the African and Eurasian plates, which are converging in the region at an estimated rate of about 4–5 mm/yr.

The Granada basin is situated over the contact area between the Internal and External Zones: its southern part is located on the Internal Zone while the northern one is on the Betic External Zone. This basin occupies the central sector of the Betic Cordillera, one of the most seismically-active areas in the Iberian Peninsula (Fig. 1), accompanied by significant active tectonics. Granada is the most populated city of the central Betic Cordillera. For these reasons, ground deformation monitoring is crucial in order to assess and mitigate seismic hazards.

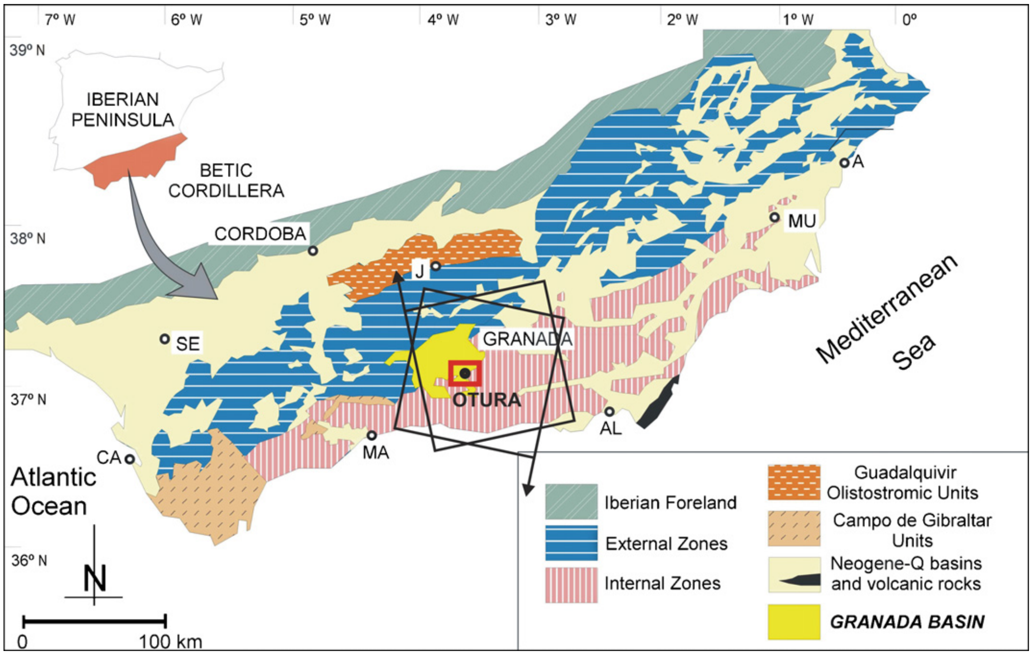

Fig. 1. Location on a geological map of the Betic Cordillera (southern Spain), situation of the Granada Basin area (small box around the Otura village) and the ascending/descending frames used in the study (black rotated boxes).

Small-magnitude earthquakes characterize the instrumental seismic activity documented in the region (Fig. 2). Occasionally there have been seismic series and seismic swarms, characterized by small-magnitude earthquakes, some moderate. Generally these are not related to a large earthquake (Galindo-Zaldívar et al., 1999), but there are some exceptions, perhaps exceeding magnitude 6, as with an earthquake which occurred on 25th December, 1884. In the Granada basin, the earthquakes have been mainly distributed in the upper crust, at a depth of between 9 and 16 km in the eastern part, and between 9 and 25 km in the western part (Morales et al., 1997).

3. Satellite datasets

The Granada basin and its surroundings are covered by a total of 22 Envisat SLCI scenes from ascending satellite track 187 and frame 729, and 29 ERS-1/2 SLCI scenes from descending satellite track 280 and frame 2853 (see locations in Fig. 1). The SAR images covered the time period from October 1992 to December 2000 (ERS-1/2) and from October 2002 to July 2006 (Envisat).

A Shuttle Radar Topography Mission (SRTM) C-band DEM with resolution of 3 arc-seconds (90 m) was used as an external DEM in this study to remove the topographic phase from the differential

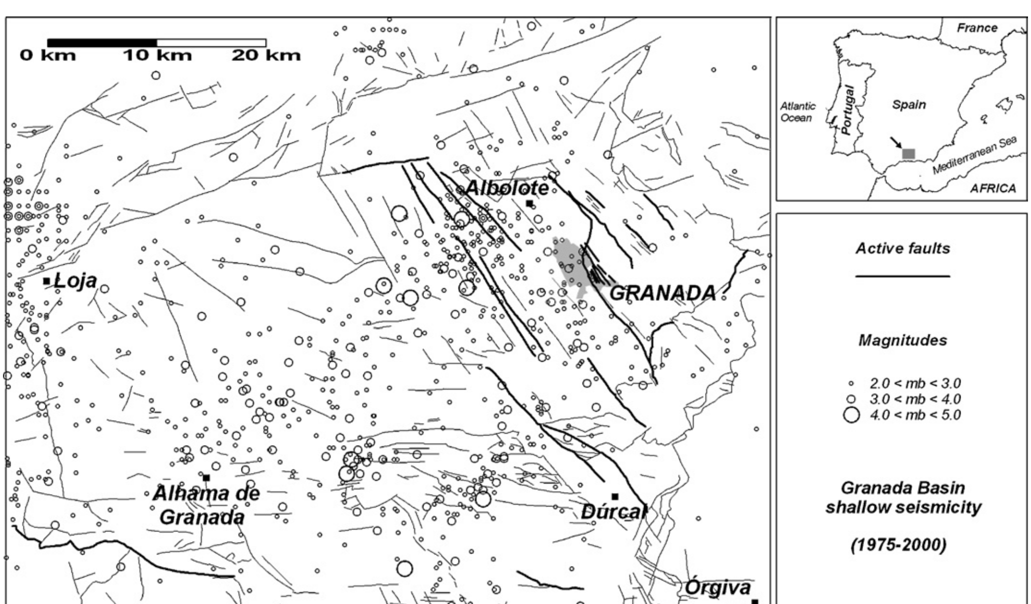

Fig. 2. Map showing epicenters and active faults in the Granada Basin and its surrounding area, from Peláez et al. (2003).

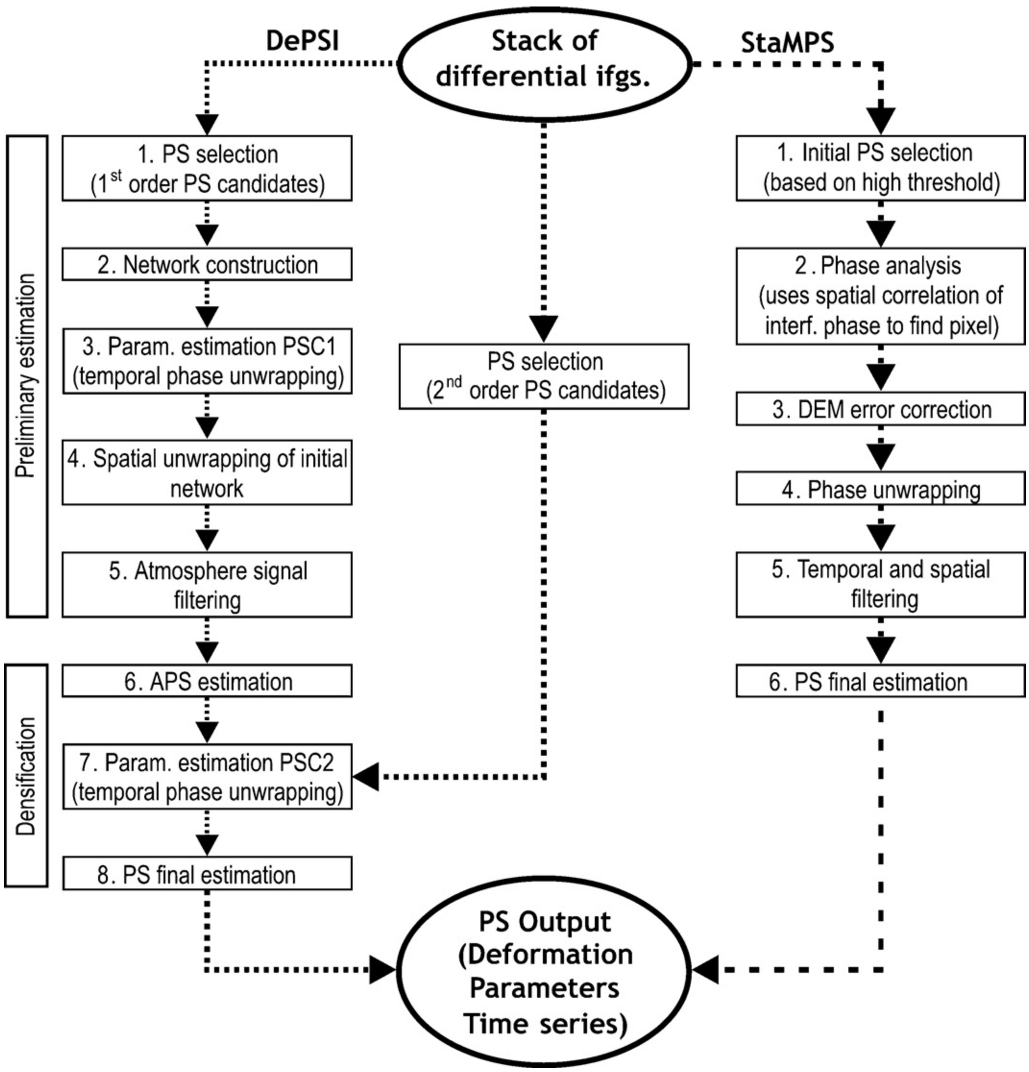

Fig. 3. DePSI and StaMPS comparative PS-InSAR flow diagram of the processing chain.

interferograms. Precise orbit data for ERS-1/2 and Envisat satellites, which enable the removal of the reference phase from the differential interferograms were provided by TU Delft (Scharroo and Visser, 1998).

4. Methodology

The idea behind PS-InSAR is to discern coherent radar signal from incoherent contributions in order to obtain only those obser-

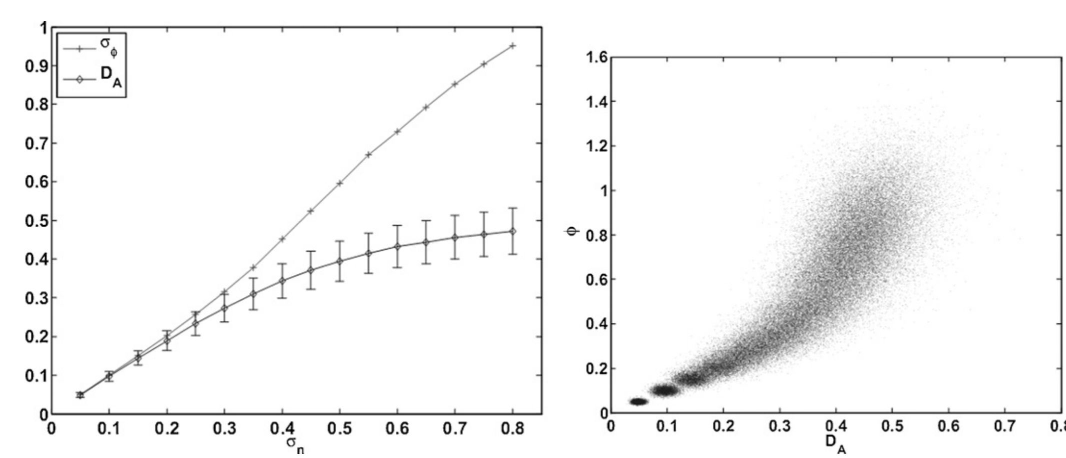

Fig. 4. Simulation of the amplitude dispersion index. A complex variable $z = s + n$ is simulated at 5000 points. The signal was fixed to $s = 1$, while the noise standard deviation (σ_n) of n was gradually incremented from 0.05 to 0.8. 33 interferograms are supposed to be available. For each value of σ_n, 5000 estimates of $\hat{\sigma}_\phi$ and $\hat{D}_A$ were calculated. (a) The mean estimated dispersion D_A (diamonds) and their standard deviations are plotted as function of the noise standard deviation, together with the phase standard deviation (plus marks) as in Ferretti et al. (2001). (b) $\hat{\sigma}_\phi$ and $\hat{D}_A$ are plotted as a scatterplot, for all values of σ_ϕ, as in Hooper et al. (2007).

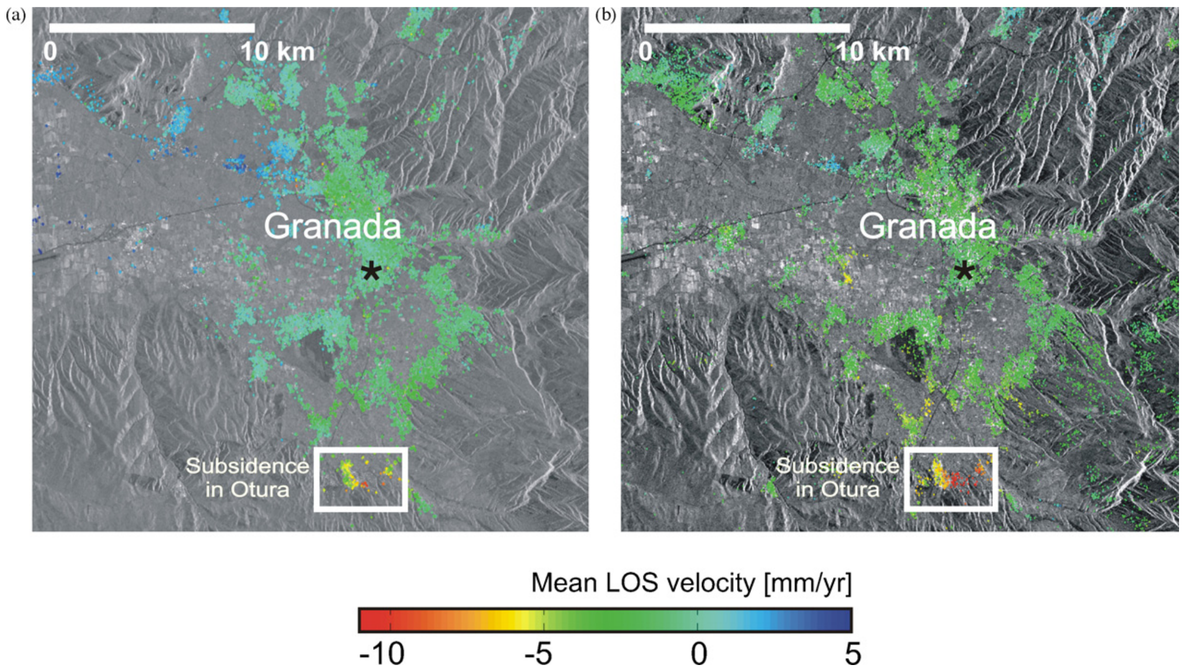

Fig. 5. ERS-1/2 stack PS-InSAR results using: (a) DePSI and (b) StaMPS. A mean amplitude image is used as background. The reference point is indicated by the black asterisk. The areas marked with a small white box represent the highest deformation rates (Otura village) and are enlarged in Fig. 6.

vations which are physically interpretable. In other words, a PS is an isolated point with interpretable phase characteristics in time. Methods for identifying and isolating these PS in interferograms have been developed using a functional model of how deformation varies with time, having been very successful in identifying PS pixels in urban areas undergoing primarily steady-state or periodic deformation.

In this section the algorithms used for PS-InSAR processing in this study are described. Fig. 3 shows a comparative flow diagram of the processing chain related to both methodologies: DePSI and StaMPS. A detailed description of both methodologies can be found in Kampes (2005), Ketelaar (2008), and Hooper et al. (2007). However, in order to explain basic concepts to the reader a short description is presented in this section.

In both approaches the input of the PSI process is a stack of differential interferograms coregistered to a selected master scene. The master is selected in order to maximize the (predicted) total coherence of the interferometric stack, based on the perpendicular and temporal baselines and the mean Doppler centroid frequency difference.

4.1. DePSI approach

To initiate the DePSI algorithm, a first set of potential PS is selected. These PS should preferably have a stable phase behaviour in time. Because the observed wrapped interferometric phases do not enable the identification of stable points, and the amount of pixels to be tested is not adequate, approximation methods are used. One option is to use the scatterer's intensity as a proxy. Fig. 4 shows that there is no linear relation between the amplitude dispersion and phase standard deviation for large values. Low SNR tends to an amplitude dispersion of 0.5 rad (Ferretti et al., 2001; Kampes, 2005). However, pixels with small amplitude dispersion are expected to have small phase standard deviation. This makes the threshold on the amplitude dispersion a useful tool of selecting pixels with expected small phase variances. Based on the amplitude dispersion D_A of a pixel, the PS selection creates a set of Persistent Scatterer Candidates (PSCs). The goal of this selection is to estimate the atmospheric phase at these pixel positions in all interferograms.

The main objective of selection of first order PS candidates (PS1c) is to establish a reference network of coherent points, which are preferably distributed homogeneously over the area of interest in order to interpolate the estimated atmospheric signal. After the calculation of relative phase observations per arc, the phase ambiguities are resolved together with the estimation of the parameters of interest. These parameters are for example the height differences and relative deformation parameters.

After ambiguity and parameter estimation per arc the parameters of interest remain relative in space, so they should be spatially integrated with respect to a single reference point (reference PS) in order to obtain absolute values. Due to noise and model imperfections, residues will be presented after integration. The unwrapping errors can be identified and rejected using the spatial network. Arcs with a questionable precision are rejected. This precision can be deduced from, for example, low temporal ensemble coherence or large least-squares residues. The measure of the variation of the residual phase for a pixel (x, y) is defined as:

$$\gamma_{x,y} = \frac{1}{N} e^{(j \cdot \varphi_{\mathrm{error}_{x,y}})} \qquad (1)$$

where $\gamma_{x,y}$ resembles the estimate of the ensemble coherence, N is the total amount of interferograms and j is the imaginary number. The residual, $error_{x,y}$ is the difference between the modelled and observed phase at location (x, y) in the observed interferogram based on Eq. (1).

Assuming that all ambiguities are estimated correctly, the integration with respect to the reference point can be carried out simply by path integration of temporally unwrapped phases without residues.

As well as phase contributions due to topography and deformation, the unwrapped phases will also contain an atmospheric delay phase. Assuming correct estimation of the topography and modelled deformation (e.g., steady state, polynomial, or periodic), the atmospheric contribution will be included in the residual phase, together with unmodelled deformation, orbit errors, and noise. The objective of the filtering step is to separate the

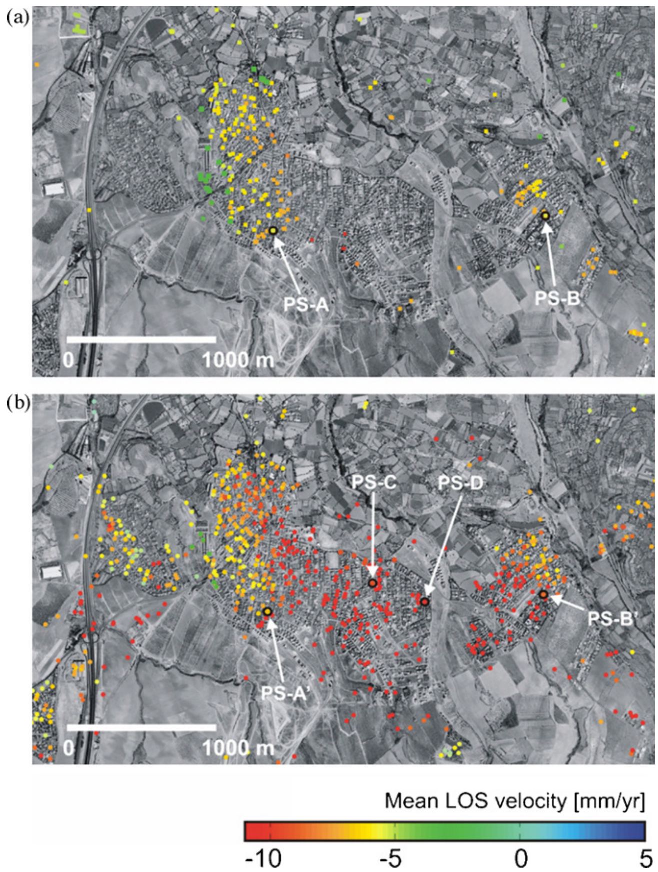

Fig. 6. PS distribution over Otura village returned by: (a) DePSI and (b) StaMPS. Some PS are selected in each image inside the subsidence bowl and their time series are represented in Fig. 7. A 0.5 m resolution ortophoto is used as a background.

atmospheric (and orbit) contribution from the unmodelled deformation.

After separation of the atmospheric phase contribution of the PS1c, the atmospheric signal for the whole scene is estimated for each interferogram using interpolation (Kriging). The result is known as atmospheric phase screen (APS).

Once all the interferograms are corrected for atmospheric effects, the ambiguities and parameters of interest are estimated for all second order PS candidates (PS2c). Each PS2c is estimated relative to the closest PS1c. After estimation of the unknown parameters and integer ambiguities, the corresponding PS candidate is tested and a final set of PS is selected.

4.2. StaMPS approach

StaMPS uses amplitude dispersion to select a subset of pixels that includes almost all of the PS pixels in the dataset. The threshold value used is consequently higher, typically in the order of 0.4. Having selected a subset of pixels as initial PS candidates, StaMPS estimates the phase stability for each of them using phase analysis. Once algorithm has converged on estimates for the phase stability of each pixel, those most likely to be PS pixels are selected, with a threshold determined by the fraction of false positives deemed acceptable. Pixels that persist only in a subset of the interferograms and those that are dominated by scatterers in adjacent PS pixels are also rejected. A phase stability indicator, γ_x, is defined based on the temporal coherence and can be used to evaluate whether the pixel is a PS

$$\gamma_x = \frac{1}{N}\left|\sum_{i=1}^{N}\exp\{j(\varphi_{\mathrm{int},x,i}-\bar{\varphi}_{\mathrm{int},x,i})-\Delta\hat{\varphi}_{h,x,i}\}\right| \tag{2}$$

where N is the number of interferograms and $\Delta\hat{\varphi}_{h,x,i}$ is the estimate of the wrapped phase $\varphi_{\mathrm{int},x,i}$ of the xth pixel in the ith *flattened* and topographically corrected interferogram. After every iteration, the root-mean-square change in coherence, γ_x, determined as in Eq. (2) is calculated. When this ceases to decrease, the solution has converged and the algorithm stops iterating. Then pixels are selected based on the probability that they are PS pixels, considering their amplitude dispersion, as well as γ_x (see Hooper et al., 2007 for details).

Once the PS have been selected, their phase is corrected for DEM error by subtracting the estimated values. As long as the density of PS is such that the absolute phase difference between neighbouring PS, after correction for estimated DEM error, is generally less than π, the corrected phase values can now be unwrapped.

Again, only the fractional phase is measured and not the integer number of cycles from satellite to the earth's surface: the phase observations are "wrapped". The first "interpretable" PS-InSAR observation is the double-difference between master and slave for two nearby PS (Hanssen, 2004). The double-difference is both a temporal and a spatial difference. This implies that StaMPS also requires a spatial and a temporal reference: one acquisition time (master image) and one reference PS.

After unwrapping, high-pass filtering is applied to unwrapped data in time followed by a low-pass filter in space in order to remove the remaining errors.

Finally, subtracting this signal leaves only deformation and spatially uncorrelated errors which can be modelled as noise.

5. Results

The processing algorithms (DePSI and StaMPS) described in Section 4 were applied to the dataset presented in Section 3.

Both ERS-1/2 and Envisat data were used, although only ERS-1/2 results are presented in this paper due to the similarity of the Envisat results.

Delft Object-oriented Radar Interferometric Software (Doris) (Kampes and Usai, 1999; Kampes et al., 2003) was used for InSAR processing with both approaches, using the DEOS precise orbits (Scharroo and Visser, 1998).

Regarding the PS-InSAR processing, a number of parameters are of importance:

For DePSI, the amplitude dispersion threshold for the selection of the initial PS was set to 0.25, using a grid size of 100 m in order to assure the minimal PS density for Atmospheric Phase Screen (APS) estimation, due to the roughness and low coherence of the terrain. This initial set of points (PS candidates) should provide spatial coverage of at least 3–4 candidates/km^2 (Colesanti et al., 2003).

During the selection of the initial PS set, very few candidates appeared outside urban areas. Possible causes may be related to the physical characteristics of the area, which induce geometric distortions and subsequent coherence loss. For the additional potential PS this threshold was 0.4.

StaMPS selects the initial set of candidates in a different way. Instead of selecting only the most stable pixels almost all of the PS pixels in the dataset are used. However, the noisiest pixels should not exceed 10% of the total. In order to make the comparison with DePSI results realistic a threshold of 0.4 was used and the unwrapping grid cell size was set to 100 m.

To enable a direct comparison between the various results, a constant colour scale was used for all figures, and the same reference point was used for all homologous processing. As the relative

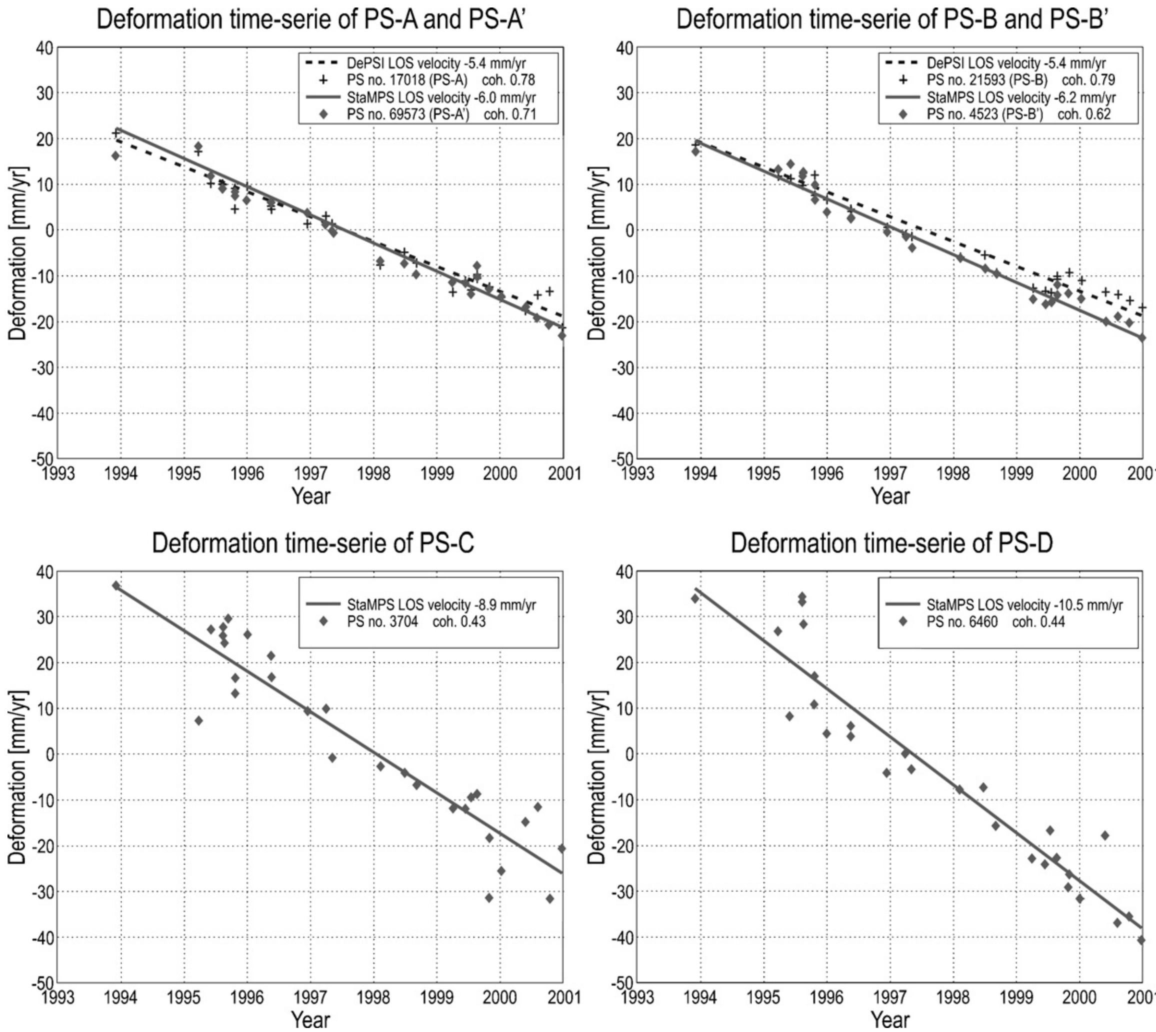

Fig. 7. Displacement time series of the selected PS in Fig. 6 with respect to the reference point (represented in Fig. 5). PS-A and PS-B are returned by DePSI and PS-A′, PS-B′, PS-C and PS-D by StaMPS. PS-A and PS-A′, and PS-B and PS-B′ are located in nearby positions respectively.

deformation precision is independent from the selected reference point this point was chosen 'arbitrarily', based on maximum phase coherence in the DePSI processing, and subsequently using the same point in the StaMPS homologous processing.

Despite the different methods used, the derived deformation rates and patterns match well (Fig. 5). The main differences between both approaches are related to the PS density and distribution. Zooming in around the area that presents the most significant deformation located over Otura (white rectangle in Fig. 5), it is clear that DePSI detects much fewer PS in the centre of the subsidence bowl (Fig. 6a) when compared with StaMPS (Fig. 6b).

There may be several reasons for these differences, the most plausible being related to the deformation rates. If these are non-linear in time, it would make the DePSI assumptions less realistic.

These observations motivated a comparative study in order to find the causes of these differences. To make the comparison easier, the same area was used in all processing even considering that the size of the area should not affect PS density, and the same setup parameters were used (when possible) in all processing.

As was explained in Section 4, the main difference between both methodologies lies in the effect of the temporal smoothness assumptions (DePSI) versus spatial smoothness assumptions (StaMPS) for PS selection. In Fig. 7, some time series plots, corresponding to the PS located inside the subsidence area, are shown (position of the PS points given in Fig. 6). DePSI PS time series are quite linear as expected due to the linear assumption used. PS time series of the points only selected by StaMPS (PS-C and PS-D), despite the linear behaviour shown, present a high level of noise. This may be the explanation to the fact that DePSI missed these PS.

The estimated displacement rates and the quality of the compared PS (A–A′ and B–B′) are listed in Table 1, for both DePSI and StaMPS. A bias of the difference between both estimates can be due

Table 1
Line-of-sight (LOS) displacement rates estimated with DePSI and StaMPS of the two common PS given in Fig. 6. A bias of the difference between both estimates can be due to the particular way that StaMPS defines the reference point (see Hooper et al., 2007 for more details).

PS	Latitude	Longitude	DePSI		StaMPS		$vel^{DePSI} - vel^{StaMPS}$ (mm/yr)
			Vel (mm/yr)	coh	Vel (mm/yr)	coh	
A	37.08574	−3.63459	−5.4	0.78	−6.0	0.71	+0.6
B	37.08676	−3.61662	−5.4	0.79	−6.2	0.62	+0.8

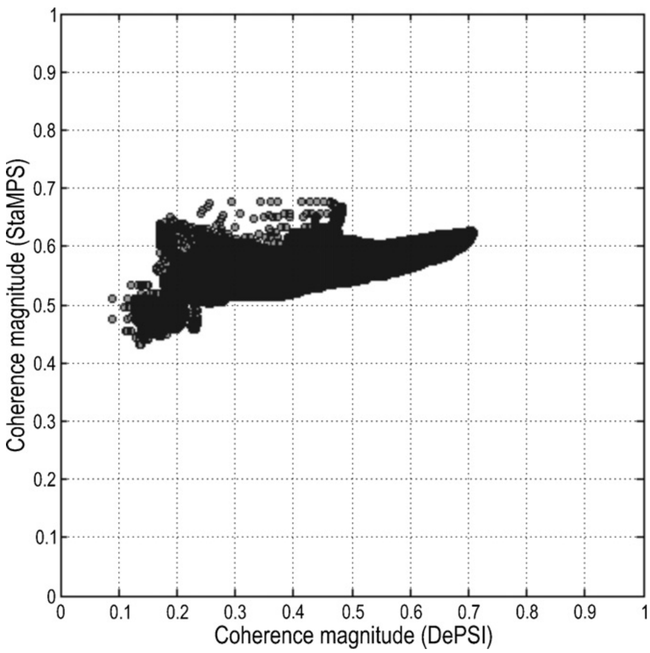

Fig. 8. Comparison of coherence magnitude of common pixels (PS) on Otura village selected by both methodologies.

to the particular way that StaMPS defines the reference point (see Hooper, 2009 for more details).

The distribution of coherence values could provide some clues to explain the different results provided by both PS-InSAR methods. Coherence can be interpreted as the average closeness of the PS phase to a given model. In StaMPS, the model is the phase interpolated from surrounding pixels (coherence is computed using Eq. (2)). In DePSI, the model is the best-fit DEM error and steady-state velocity, plus atmosphere and orbit errors interpolated from a network of PS (coherence is computed using Eq. (1)). Fig. 8 shows a comparison of coherence magnitude for all pixels selected as PS by both methods around the Otura village. For this subset of pixels, common to both methods, the observed phase is generally closer to the model in StaMPS than in DePSI.

6. Discussion

In the scope of this comparative study, ground motion processes have been identified for the first time in the area of our analysis using PS-InSAR, the most significant being a subsidence bowl located over the village of Otura. Two major causes were identified to explain this unexpected phenomenon: fast infrastructural developments taking place in the village (e.g., new residential areas and new highways) leading to soil compaction; and intensive extraction of underground water originated by the increase of population in the last years (Sousa et al., 2008). The absence of external data (GPS, levelling, etc.) in the past or a geological model makes an effective quantitative validation of this deformation non-viable. For this purpose, there are plans for establishing a levelling network in the area.

As expected, the highest densities of PS relate to urban areas, where coherently scattering objects exist. With the current settings, StaMPS is better able to find persistent scatterers in areas of forest, agriculture or mountains (Fig. 5). For the Otura (subsidence area), a different PS density (Fig. 6) is the most significant difference.

It has to be noted that all deformation maps must be interpreted in a relative sense. There is no absolute deformation to be derived from PS-InSAR measurements. As the PS measurements are relative to a reference point, the precision of the estimates is high. However, the absolute localization accuracy of the scatterers is relatively poor due to orbit uncertainty, instrumental and propagation delays, and scattering centre uncertainty.

The trade-off between data density and data quality follows clearly when comparing the coherence histograms of both approaches. Whether the differences are due to threshold settings, complex deformation behaviour or urban development could not yet be assessed.

The main differences in the methodologies are related to both interferometric and PS-InSAR processing. Like DePSI, StaMPS uses Doris for all the interferometric processing. There are, however, some differences between both approaches: StaMPS does not apply oversample, and the coregistration procedure is also different. In order to avoid decorrelation problems motivated, for example, by large temporal and spatial baselines, StaMPS uses an amplitude based algorithm to estimate offsets in position between pairs of images with good correlation. The function that maps the master image to every other image is then estimated by weighted least-squares inversion (Hooper et al., 2007). These differences could be significant, mainly when areas of low coherence are processed.

In the PS-InSAR processing there are also some important differences, mainly, in the PS selection criterion, atmosphere estimation and unwrapping.

7. Conclusion

The expected slow/moderate active tectonics associated with this sector of the Eurasian–African plate boundary, Granada basin, was confirmed by both the DePSI and StaMPS approaches. Moreover, anthropogenic effects caused by urban expansion and intensive water extraction, have been detected, proving once again the utility of InSAR techniques for detecting anthropogenic phenomena and eventually continuous monitoring.

Depending on the PS-InSAR methodology applied different results can be achieved (PS density and location). We conclude that StaMPS has better behaviour compared to DePSI when applied to areas with non-linear deformation. However, when applied to relatively stable urban areas like Granada city, similar results are provided by both approaches. The DePSI linear deformation assumption parameter seems to be, in this case, sub-optimal, and therefore explains the lower phase residual coherence in the subsidence bowl area.

Both approaches provide identical deformation rates and are able to detect even weak deformation rates. StaMPS, however, due to its spatial smoothness assumption is particularly adequate to monitor and detect spatially correlated deformation. In contrast, DePSI, due to its temporal smoothness assumptions is adequate to detect pixels associated to isolated movements. When the area of interest is mostly composed of urban areas, DePSI is the most appropriate method. In the other cases, StaMPS is more desirable.

A future pixel-level comparison will explain how each approach used in this work selects the PS in order to take advantage of each method's specificities in working towards their possible integration.

Acknowledgments

The authors are grateful to two anonymous reviewers for their valuable comments and suggestions. This research was supported by the European Space Agency (ESA) in the scope of 3858 and 3963 CAT-1 projects, the PR2006-0330, ESP2006-28463-E, CSD2006-00041, and CGL 2006-06001 projects from Ministerio de Educación y Ciencia (Spain), the RNM-149 and RNM-282 research groups of the Junta de Andalucía (Spain) and Fundação para a Ciência e a Tecnologia (Portugal). TUDelft radar group and Stanford University are gratefully acknowledged for all the technical support. The SRTM data were provided by USGS/NASA.

References

Colesanti, C., Ferretti, A., Prati, C., Rocca, F., 2003. Monitoring landslides and tectonic motions with the permanent scatterers technique. Eng. Geol. 68, 3–14.

Ferretti, A., Prati, C., Rocca, F., 1999. Permanent scatterers in SAR interferometry. In: IEEE Proceedings on Geoscience and Remote Sensing Symposium, IGARSS'99, June 28–July 2, 3, pp. 1528–1530.

Ferretti, A., Prati, C., Rocca, F., 2000. Nonlinear subsidence rate estimation using permanent scatters in differential SAR interferometry. IEEE T. Geosci. Remote 38 (5), 2202–2212.

Ferretti, A., Prati, C., Rocca, F., 2001. Permanent scatters in SAR interferometry. IEEE T. Geosci. Remote 39 (1), 8–20.

Gabriel, A.K., Goldstein, R.M., Zebker, H.A., 1989. Mapping small elevation changes over large areas: differential radar interferometry. J. Geophys. Res. 94 (B7), 9183–9191.

Galindo-Zaldívar, J., González-Lodeiro, F., Jabaloy, A., 1993. Stress and palaeostress in the Betic-Rif cordilleras (Miocene to the present). Tectonophysics 227, 105–126.

Galindo-Zaldívar, J., Jabaloy, A., Serrano, I., Morales, J., González-Lodeiro, F., Torcal, F., 1999. Recent and present-day stresses in the Granada Basin (Betic cordilleras): example of a late Miocene-present-day extensional basin in a convergent plate boundary. Tectonics 18, 686–702.

Hanssen, R.F., 2001. Radar Interferometry: Data Interpretation and Error Analysis. Kluwer Academic Publishers, Dordrecht, The Netherlands.

Hanssen, R.F., 2004. Stochastic Modeling of Times Series Radar Interferometry. In: International Geoscience and Remote Sensing Symposium. IGARSS'04, Anchorage, Alaska, 20–24 September.

Hanssen, R.F., Feijt, A., 1996. A first quantitative evaluation of atmospheric effects on SAR interferometry. In: 'FRINGE 96' Workshop on ERS SAR Interferometry, Zürich, Switzerland, 30 September–2 October, ESA SP-406, pp. 277–282.

Hooper, A., Segall, P., Zebker, H., 2007. Persistent scatterer InSAR for crustal deformation analysis, with application to Volcán Alcedo, Galapagos. J. Gephys. Res. 112, B07407, doi: 10.1029/2006JB004763.

Hooper, A., 2009. StaMPS/MTI Manual, version 3.1. Delft Institute of Earth Observation and Space Systems. Delft University of Technology, The Netherlands.

Kampes, B.M., Hanssen, R.F., Perski, Z., 2003. Radar interferometry with public domain tools. In: FRINGE 2003 Workshop, ESA/ESRIN, Frascati, Italy.

Kampes, B.M., 2005. Radar Interferometry: Persistent Scatterer Technique. Kluwer Academic Publishers, Dordrecht, The Netherlands.

Kampes, B.M., Usai, S., 1999. Doris: the delft object-oriented radar interferometric software. In: Proceedings of the 2nd International Symposium on Operationalization of Remote Sensing, Enschede, The Netherlands.

Ketelaar, V.B.H., 2008. Monitoring surface deformation induced by hydrocarbon production using satellite radar interferometry. PhD thesis, Delft University of Technology, Delft, The Netherlands.

Massonnet, D., Feigl, K.L., 1998. Radar interferometry and its application to changes in the earth's surface. Rev. Geophys. 36 (4), 441–500.

Monti Guarnieri, A., Tebaldini, S., 2007. Hybrid Cramér-Rao bounds for crustal displacement field estimators in SAR Interferometry. IEEE Signal Proc. Lett. 14 (12), 1012–1015.

Morales, J., Serrano, J., Vidal, F., Torcal, R., 1997. The depth of the earthquake activity in the Central Betics (Southern Spain). Geophys. Res. Lett. 24, 3289–3292.

Peláez, J.A., Sanz de Galdeano, C., López-Casado, C., 2003. Use of active fault data versus seismicity data in the evaluation of seismic hazard in the Granada Basin (southern Spain). B. Seismol. Soc. Am. 93 (4, August), 1670–1678.

Sanz de Galdeano, C., Vera, J.A., 1992. Stratigraphic record and palaeogeographical context of the Neogene basins in the Betic Cordillera, Spain. Basin Res. 4, 21–36.

Scharroo, R., Visser, P., 1998. Precise orbit determination and gravity field improvement for the ERS satellites. J. Geophys. Res. 103 (C4), 8113–8127.

Sousa, J.J., Ruiz, A.M., Hanssen, R.F., Perski, Z., Bastos, L., Gil, A.J., 2008. PS-INSAR measurement of ground subsidence in Granada area (Betic Cordillera, Spain). In: Proceedings of the 13th FIG International Symposium on Deformation Measurements and Analysis, Lisbon, Portugal, 12–15 May, Lisbon, Portugal.

Usai, S., 1997. The use of man-made features for long time scale INSAR. Geoscience and Remote Sensing, 1997. In: IGARSS '97. Remote Sensing—A Scientific Vision for Sustainable Development, 1997 IEEE International, 4, pp. 1542–1544.

Usai, S., Hanssen, R., 1997. Long time scale INSAR by means of high coherence features. In: Proceedings of the 3rd ERS Symposium on Space at the service of our Environment, Florence, Italy, 14–21 March, European Space Agency.

Zebker, H.A., Rosen, P.A., Hensley, S., 1997. Atmospheric effects in interferometric synthetic aperture radar surface deformation and topographic maps. J. Geophys. Res. 102 (B4), 7547–7563.